JACS
JOURNAL OF THE AMERICAN CHEMICAL SOCIETY
pubs.acs.org/JACS
Article

$[Co_3@Ge_6Sn_{18}]^{5-}$: A Giant σ-Aromatic Cluster Analogous to H_3^+ and Li_3^+

Ya-Shan Huang, Hong-Lei Xu, Wen-Juan Tian, Zi-Sheng Li, Sílvia Escayola, Miquel Solà, Alvaro Muñoz-Castro, and Zhong-Ming Sun*

Cite This: https://doi.org/10.1021/jacs.4c16401
Read Online
ACCESS | Metrics & More | Article Recommendations | Supporting Information

ABSTRACT: Aromaticity is one of the most important concepts in chemistry and has been successfully extended to all-metal clusters. However, the study of all-metallic aromatic clusters remains in its early stages, with σ-aromatic clusters mostly limited to small sizes ($\leq$12) that often require external stabilization. In this work, we report the first Ge/Sn-based trimer, $[Co_3@Ge_6Sn_{18}]^{5-}$, which can be rationalized as the fusion of three $[Co^-@Ge_3Sn_6^{4-}]$ units via a Ge_3 face. Theoretical studies have revealed that two σ-electrons are delocalized across the entire trimer, with the spherical aromaticity of each $[Co@Ge_3Sn_6]$ unit and the global σ-aromaticity of $[Co_3@Ge_6Sn_{18}]^{5-}$ further supported by its electron delocalization and magnetic behavior. As a result, this trimer can be viewed as a giant σ-aromatic counterpart to triatomic H_3^+ and Li_3^+. Our findings suggest the potential for synthesizing cluster-of-cluster analogs of discrete all-metallic aromatic species, such as Al_4^{2-}, and further enhance our understanding of chemical bonding.

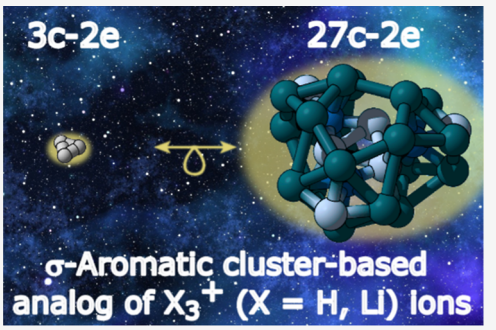

INTRODUCTION

Since the discovery of benzene,[1,2] the concept of aromaticity has profoundly advanced our understanding of the electronic structure and stability of compounds.[3] Aromaticity has become one of the most significant concepts in chemistry.[4] Over the past few decades, this concept has expanded beyond the original π-electron delocalization system to include other types of electrons, such as σ-electrons. σ-Aromaticity was first introduced to explain the anomalous magnetic properties of cyclopropane.[5,6] Aromaticity has also transcended the realm of planar organic compounds, extending to inorganic compounds with diverse structures,[7−11] thereby opening the door to new forms of aromaticity, including 3D aromaticity.[12−14] Substantial efforts have been devoted to predicting aromaticity through theoretical calculations.[15,16] A notable example is Li_3^+, an H_3^+ analog with two σ-electrons delocalized over the simplest all-metal cluster,[17−22] although there is less consensus about its σ-aromaticity (Figure 1a).[20] The limits of theoretical models pose significant obstacles to the accurate prediction and ultimate synthesis of all-metal aromatic clusters, particularly with regard to the need to consider electron correlation, as well as relativistic and environmental effects in the calculations.[15,16] Typical isolable clusters include onion-like $[E@M_{12}@E_{20}]^{n-}$ (E = As, M = Ni, n = 3; E = Sb, M = Pd, n = 3, 4; E = Sn, M = Cu, n = 12; E = Bi, M = Pb, n = 6),[23−27] and the all-metal fullerene $[K@Au_{12}Sb_{20}]^{5-}$,[28] which exhibit 3D aromaticity.[29] Despite these advances, the synthesis of all-metal aromatic compounds remains in its infancy. Most known all-metal aromatic compounds are limited to small systems, often requiring external stabilization, such as the σ-aromatic $[Au_3]^+$ in $[(NHC^{Dipp}Au)_3]^+$,[30] $[Zn_3]^+$ in $[Zn_3Cp^*_3]^+$,[31] and $[Bi_4]^{4+}$ in $[(Bi_4)(EtCxInBr)_2]$ (Figure 1b).[32] From a theoretical point of view, $[Cu_3]^+$ is also considered a σ-aromatic cluster.[33,34] Recently, a Th_3 cluster has been reported, which shows σ-aromaticity for actinides (Figure 1b), despite doubts raised by Foroutan-Nejad and Szczepanik.[35−39] The relatively larger clusters, $[M@Au_{12}]^{6+}$ (M = Pd, Pt) (Figure 1b), found within the ligand-protected $[MAu_{24}(SR)_{18}]$ clusters also exhibit σ-aromaticity and adopt an icosahedral structure.[40] Additionally, although several large aromatic clusters have been reported, their aromaticity originates from smaller aromatic building blocks. Some of these clusters incorporate a σ-aromatic plane, such as $[AuSb_4]$ in $[Au_2Sb_{16}]^{4-}$,[41] $[Sn_3]$ in $[As_3Nb(As_3Sn_3)]^{3-}$,[42] and $[M_2Sb_2]$ (M = Cu, Ag) in $[(MSn_2Sb_5)_2]^{4-}$ (Figure 1c).[43] Furthermore, clusters such as $[Ge_{24}]^{4-}$,[44] $\{(Ge_9)_2[\eta^6\text{-}Ge(PdPPh_3)_3]\}^{4-}$,[45] and $[Sn_{36}]^{8-}$,[46] feature multiple local σ-aromatic E_9 (E = Ge, Sn) fragments.[47] In this work, we successfully isolated and structurally characterized the first Ge/Sn-based trimer, $[Co_3@Ge_6Sn_{18}]^{5-}$ (**1a**), formed by the fusion of three $[Co@Ge_3Sn_6]$ units through a $[Ge_3]$ face. Notably, **1a** is distinguished by a

Received: November 19, 2024
Revised: February 25, 2025
Accepted: February 26, 2025

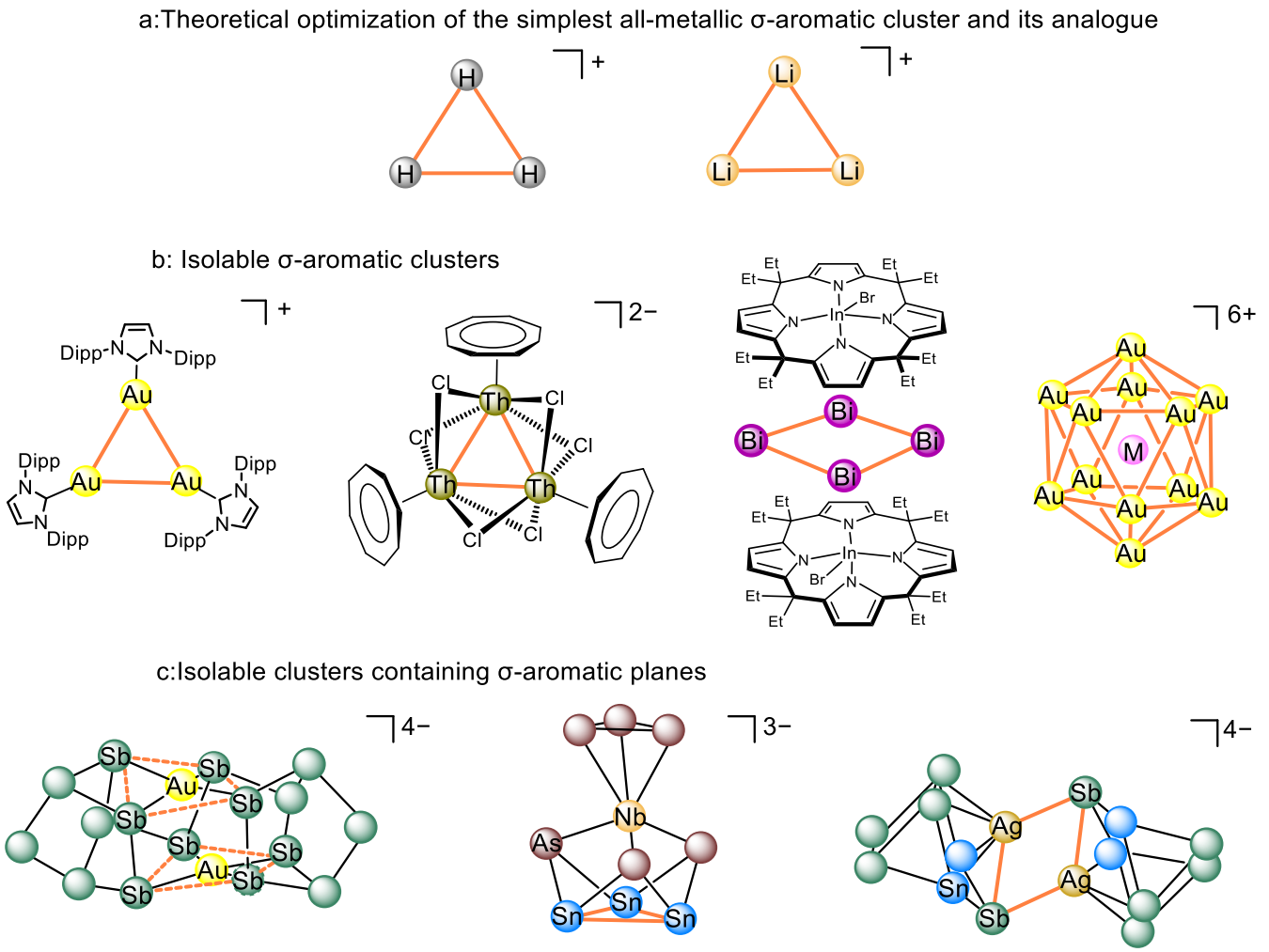

Figure 1. Selected examples of σ-aromatic clusters. The units composed of orange bonds indicate the presence of aromaticity.

$[Co_3Ge_3]$ unit featuring a benzene-like ring with six exceptionally short sides. Theoretical calculations revealed that **1a** can be described as a 2e σ-bonded trimer, representing a giant σ-aromatic counterpart to the triatomic σ-aromatic H_3^+ and Li_3^+, thus extending the analogy between prototypical molecules and cluster-based aggregates.

RESULTS AND DISCUSSION

To date, research on group 14 clusters has focused primarily on the reactivity of homoatomic E_9^{4-} (E = Si, Ge, Sn, and Pb), leading to the discovery of various fascinating structures, including the aforementioned Ge and Sn clusters with local aromaticity.[44−52] In contrast, mixed systems $[E1_{9-x}E2_x]^{4-}$, such as Si/Ge and Ge/Sn, have been less studied due to limited experimental conditions. Si/Ge clusters are typically formed under extreme conditions, such as in liquid ammonia.[53] Although $[Ge_{9-x}Sn_x]^{4-}$ clusters are available from the solution of the ternary precursor $K_4Ge_{4.5}Sn_{4.5}$, their solution-phase chemistry has been challenging to study because of their high reactivity, uneven charge distribution, and sensitivity to reaction conditions.[54] Only a few species derived from Ge/Sn precursors have been obtained, including functionalized clusters such as $[GeSn_8R]^{3-}$ (R = −HC = CH_2, −CH = CHCpr) (Cpr = cyclopropyl),[54] $[Ge_2Sn_7R]^{3-}$ (R = −CH = CHPh),[54] $[Ge_2Sn_7R_2]^{2-}$ (R = −CH = CH_2),[54] as well as double-cage structures such as $[(Sn_6Ge_2Bi)_2]^{4-}$,[55] and $[\{Ni@Sn_8(\mu-Ge)_{1/2}\}_2]^{4-}$.[56] These Ge/Sn clusters share a common characteristic: the exobonds preferentially connect to Ge atoms rather than Sn atoms, with Ge atoms consistently serving as the common vertices instead of Sn. In this work, we describe the reaction of the ternary Zintl precursor $K_4Ge_{4.5}Sn_{4.5}$ with $Co(PPh_3)_2Cp$ in *N*,*N*-dimethylacetamide (DMA), yielding the first triple-cage Ge/Sn-mixed cluster compound, $[K(2.2.2-crypt)]_5[Co_3@Ge_6Sn_{18}]$ 2tol·DMA (**1**). Single−crystal X−ray diffraction revealed that compound **1** crystallizes in the monoclinic space group $P2_1$ and contains one cluster anion $[Co_3@Ge_6Sn_{18}]^{5-}$ (**1a**), five $[K(2.2.2-crypt)]^+$ counter−cations, one DMA molecule, and two toluene molecules (Figures S3 and S4). The anion cluster is statistically disordered at the atomic positions, displaying one major component in **1a** and a minor component (Figure S2). The following discussion focuses on the major components due to their almost identical structural characteristics. Energy-dispersive X-ray spectroscopy (EDS, Figure S39) analysis revealed that the atomic ratios in compound **1** (K/Co/Ge/Sn = 5.4:2.9:6.0:18.2) are very close to the theoretical values (Table S2). Crystals of compound **1** were dissolved in DMA or acetonitrile (ACN) for electrospray ionization mass spectrometry (ESI−MS), revealing a series of fragments with varying Ge/Sn ratios. This situation was also found in the reported Ge/Sn-mixed clusters $[GeSn_8R]^{3-}$ (R = −HC = CH_2, −CH = CHCpr).[54] Analysis of the DMA solution of compound **1** by

https://doi.org/10.1021/jacs.4c16401
J. Am. Chem. Soc. XXXX, XXX, XXX−XXX

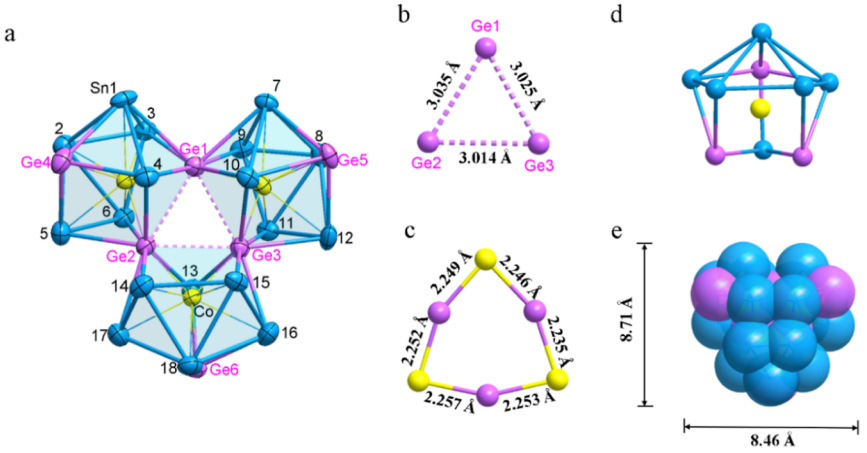

Figure 2. (a) Ellipsoid plot (50% level) of the crystal structure of $[Co_3@Ge_6Sn_{18}]^{5-}$ (**1a**); (b) equilateral triangle-shaped fragment of $[Ge_3]$; (c) benzene-like ring of $[Co_3Ge_3]$; (d) view of the $[Co@Ge_3Sn_6]$ cage; (e) space−filling representation of $[Co_3@Ge_6Sn_{18}]^{5-}$.

ESI−MS revealed a mass envelope corresponding to the parent cluster ($\{[KCo_3Ge_6Sn_{18}]\}^{2-}$, Figures S5 and S20) and fragments with various Ge/Sn ratios ($\{[KCo_3Ge_xSn_{24-x}]\}^{2-}$ (x = 7−13), Figure S5). Furthermore, significant decomposition processes in solution resulted in the formation of fragments such as $\{[Co_3Ge_xSn_{9-x}]\}^{-}$ (x = 1−7, Figure S5) and $\{[K_3Co_2Ge_xSn_{13-x}]\}^{-}$ (x = 2−6, Figure S5). In comparison, when dissolved in ACN, only smaller fragments of $\{[KCo_2Ge_xSn_{14-x}]\}^{-}$ (x = 5−9, Figure S26) and $\{[CoGe_xSn_{10-x}]\}^{-}$ (x = 1−7, Figure S26) were observed.

The 24−vertex cage can be viewed as three $[Co@Ge_3Sn_6]$ subunits fused through three germanium atoms (Ge1, Ge2, and Ge3), with an almost equilateral triangle arrangement (Figure 2a, b, and d). The Ge−Ge distances in the Ge_3 triangle are elongated to 3.025 Å (av.), exceeding the typical Ge−Ge contact range (2.4−2.7 Å),[48,49] indicating that there are no direct Ge−Ge interactions. The three $[Co@Ge_3Sn_6]$ subunits possess almost identical structures, and slight differences may be caused by the disorder of the cluster (Figure 2d). A closer look at the $[Co@Ge_3Sn_6]$ subunits reveals that, similar to C_{4v}−symmetric $[Co@Sn_9]^{5-}$,[57,58] each can be described as a distorted mono-capped square antiprism. The distances (2.235−2.257 Å) from the cobalt atoms to the shared germanium atoms (Ge1, Ge2, and Ge3) are significantly short, being shorter than the sum of the covalent radii of Co and Ge (2.38 Å for the Pauling covalent radii and 2.32 Å for the Pekka Pyykkö covalent radii).[59,60] The three cobalt atoms and three shared germanium atoms are almost in the same plane, forming a benzene-like Co_3Ge_3 ring (Figure 2c). The rest of the Co−Ge bond lengths span a range of 2.624−2.675 Å, comparable to those in $[Co_2@Ge_{16}]^{4-}$ (2.519−2.627 Å),[61] longer than those observed in $[Co@Ge_9]^{5-}$ (2.331−2.374 Å)[62] and $[Co@Ge_{10}]^{3-}$ (2.479−2.525 Å).[63] This finding indicates that the Co atoms in the cluster are slightly shifted from the center toward the fused edge. A similar situation also occurred in $[\{Ni@Sn_8(\mu-Ge)_{1/2}\}_2]^{4-}$ and $[Ni_2@Sn_{17}]^{4-}$,[56,64] where distances from the Ni atoms to the shared atoms are short, 2.227 and 2.384 Å (av.), respectively. The Co−Sn bond lengths (2.555−2.801 Å) are similar to those observed in $[Co@Sn_9]^{5-}$ (2.518−2.702 Å)[57,58] and $[Co_2@Sn_{17}]^{5-}$ (2.384−3.747 Å).[57] Ge−Sn distances involving Ge4, Ge5, and Ge6 (2.884 Å av.) are longer than those in the alkenyl-substituted Ge/Sn-mixed clusters (2.600−2.864 Å),[54] $[(Ge_9)Sn(Ge_9)]^{4-}$ (2.630−2.709 Å),[65] and $[(Sn_6Ge_2Bi)_2]^{4-}$ (2.670−2.801 Å).[55] The longest Ge−Sn distances are observed from the shared Ge atoms to the Sn atoms (2.980 Å av), likely due to the high coordination number of the shared Ge atoms. The Sn−Sn distances (3.012 Å av.) are comparable to those in $[Co@Sn_9]^{5-}$ (2.957−3.750 Å)[57,58] and fall within the typical range for tin clusters.[48]

The $[Co_3@Ge_6Sn_{18}]^{5-}$ structure features the aggregation of three $[Co@Ge_3Sn_6]$ cluster units, which act as building blocks, with an overall electron count of 128 (6×Ge + 18 × Sn + 3 × Co + 5 = 6 × 4 + 18 × 4 + 3 × 9 + 5 = 128). The Hirshfeld charge analysis exhibits a value of −0.38 e^- for $[Co_3@Ge_6Sn_{18}]^{5-}$, which is similar to the calculated for $[Co@Sn_9]^{5-}$ (−0.41 e^-), which involves a formal $[Co^-@Sn_9^{4-}]$ charge distribution.[57,58] Moreover, natural population analysis (NPA) agrees with the negatively charged Co atom of $[Co@Sn_9]^{5-}$, amounting to −1.89 e^-, and of −2.91 e^- in $[Co_3@Ge_6Sn_{18}]^{5-}$. Thus, the characterized cluster features a $[Co_3^{3-}@Ge_6Sn_{18}^{2-}]$ charge distribution involving three d^{10}-Co^- centers (30 electrons). The remaining 98 cluster electrons from the $Ge_6Sn_{18}^{2-}$cyclic trimer skeleton provided bonding electrons to retain the aggregate. In addition, the NPA carried out on the optimized structure of $[Co_3@Ge_6Sn_{18}]^{5-}$ revealed that Co_3 has a total charge of −3.08 lel, which is consistent with the aforementioned result.

Formally, each isolated building unit can be considered a $[Co@Ge_3Sn_6]^{5-}$ cluster featuring a *nido*-$[Ge_3Sn_6]^{4-}$ cage filled with a d^{10}-Co^- atom, which is isoelectronic to $[Co@Sn_9]^{5-}$.[57,58] This cage involves 40 cluster electrons in a $1S^21P^61D^{10}2S^21F^{14}2P^6$ electronic structure[66] with the addition of the d^{10}-Co^- atomic shell. Building block aggregation by oxidative coupling,[46,67,68] resulting in the formation of the overall $[Co_3@Ge_6Sn_{18}]^{5-}$ cluster, leads to a decrease in the number of available electrons. Considering the presence of three d^{10}-Co^- ions in the $[Co_3@Ge_6Sn_{18}]^{5-}$ structure, each Ge_3Sn_6 unit fused cluster shares the remaining 98 cluster electrons in terms of 32 electrons per unit (3 × 32 = 96, 32 e^- following the Hirsch rule[29] with N = 3), featuring a filled $1S^21P^61D^{10}1F^{14}$ electronic closed-shell according to the jellium model,[69−71] leaving 2 electrons to be distributed on the overall cluster. Owing to the resulting cluster aggregation, each unit is able to contribute with the 2S shell to the bonding elements in the trimer, where the 2 available 2 electrons remain in a bonding combination between the cyclic array of three 2S shells. Hence, the trimer sustains a bonding 2S + 2S + 2S

https://doi.org/10.1021/jacs.4c16401
J. Am. Chem. Soc. XXXX, XXX, XXX−XXX

combination, leading to cluster-of-cluster bonding characteristics.[72,73]

To further evaluate the electronic structure, the Boys−Foster orbitals localization (BODL) scheme[74] was carried out at the ZORA-PBE0/TZ2P level of theory (see the Supporting Information for further computational details). Lewis-like bonds (2c−2e), lone pairs (1c−2e), and multicenter (*n*c−2e) bonding elements can all be deciphered from the localized molecular orbitals (LMOs) obtained via the BODL method. Fifteen lone pairs are found, ascribed to the set of d^{10}-Co^{-} atomic orbitals (AOs) (Figure 3). For the Ge_6Sn_{18} structure,

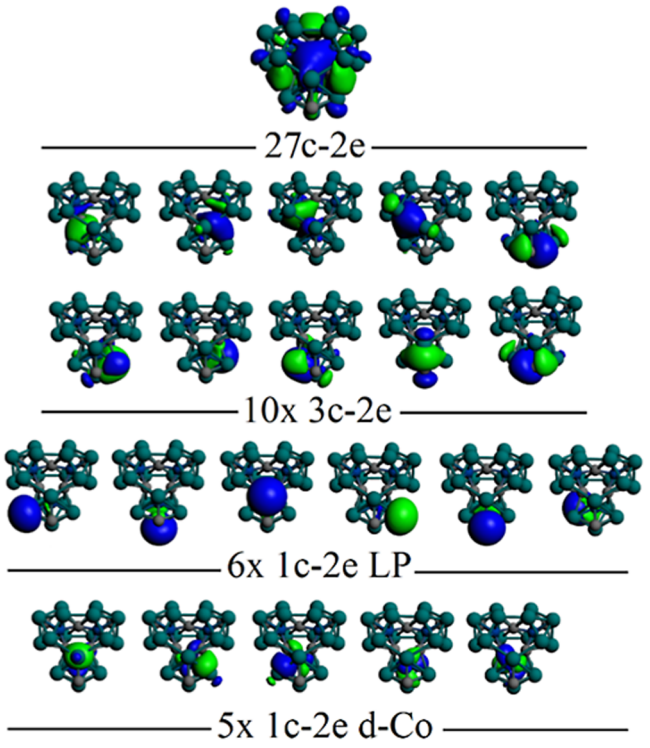

Figure 3. LMOs accounting for 27c−2e and representative LMOs at each $Co@Ge_3Sn_6$ unit.

18 lone pairs are located at each nonfused Sn and Ge vertex, six per Ge_3Sn_6 unit, with the addition of 30 3c−2e localized orbitals placed at each deltahedral face, 10 per Ge_3Sn_6 unit, accounting for the distribution from 96 cluster electrons, which are located mainly at each Ge_3Sn_6 unit. Notably, the remaining 2 electrons are placed in a multicenter 27c−2e bond, supporting the bonding interaction between three 2S shells centered at each constituent unit. Thus, the overall $[Co_3@Ge_6Sn_{18}]^{5-}$ cluster can be described as a 2e σ-bonded trimer with resemblance to triatomic species featuring a 3c−2e σ-bond, such as H_3^+ and Li_3^+ (Figure S40).[17−22] This 27c−2e bond is contributed mainly by the central Ge_3 ring involving 4p-Ge AOs (51%), 14% from central 4s-Ge AOs, and 6% from endohedral 4p-Co AOs, with 29% from peripheral 5p-Sn/4p-Ge AOs. Wiberg bond indices reveal values of 0.23 for Ge−Ge bonds in the central Ge_3 ring and 1.50 for each pair of $Co@Ge_3Sn_6$ units.

This finding suggests that the $[Co_3@Ge_6Sn_{18}]^{5-}$ cluster has aromatic characteristics on the basis of the resulting σ-bond spread on the trimer. Calculation of the global electron density of delocalized bonds[75−77] ($EDDB_G$, for the entire $[Co_3@Ge_6Sn_{18}]^{5-}$ cluster) at the PEB0/def2-TZVP level of theory yields 44.7 delocalized electrons, i.e., 1.66 e/atom, whereas the EDDB for the benzene-like ring of $[Co_3Ge_3]$ yields 1.4 electrons, 0.23 e/atom. This result indicates that the delocalization is global and involves the entire cluster rather than being localized in the $[Co_3Ge_3]$ ring (Figure S41). Moreover, to account for the overall magnetic behavior inherent to aromatic species,[78,79] NICS isosurfaces[80] and GIMIC ring currents[81,82] were obtained. In Figure 4a, the NICS isosurfaces show that three spherical-like shielding regions are placed at each Ge_3Sn_6 unit, which is a common feature of spherical aromatic clusters and indicates that spherical aromatic characteristics remain at each building block. In addition, the shielding region spreads along with the shared sections,[78,80,83,84] suggesting global aromatic behavior in the trimer. To further unravel the aromatic characteristics of $[Co_3@Ge_6Sn_{18}]^{5-}$, the plausible formation of shielding cone characteristics can be obtained from the increase in the shielding and deshielding regions under particular orientations of the external magnetic field. For a field oriented along the *z*-axis (B_z^{ind}), also noted as $NICS_{zz}$, a long-range shielding cone is unraveled involving the overall structure with a complementary deshielding region placed perpendicularly to the external field. Thus, the σ-bonded trimer is ascribed to a σ-aromatic cluster aggregate, the first example reported to date. Moreover, along the *x*- and *y*-axes (B_x^{ind} and B_y^{ind}), a similar

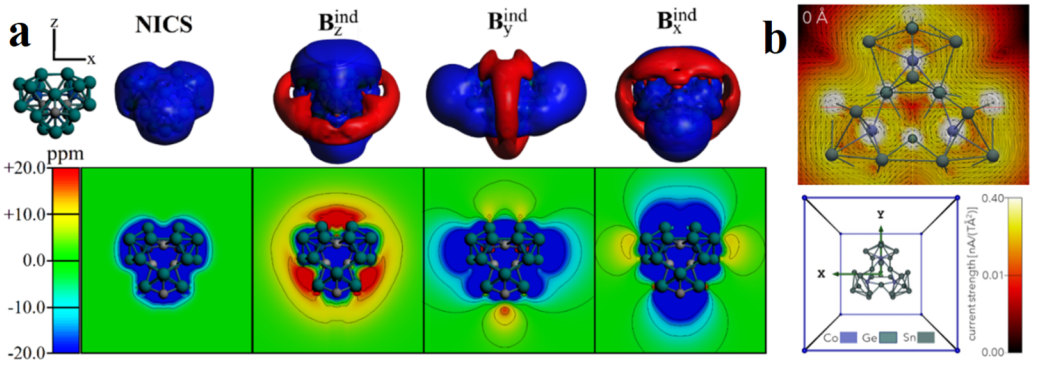

Figure 4. (a) Isosurface and contour plot representation of the magnetic response properties for $[Co_3@Ge_6Sn_{18}]^{5-}$, denoting the NICS (isotropic/averaged) term, and from different orientations of the external field (B_x^{ind}, B_y^{ind}, and B_z^{ind}). Isosurfaces set to ±8 ppm, blue: shielding; red: deshielding. (b) Current density of the $[Co_3@Ge_6Sn_{18}]^{5-}$ cluster at the central plane located at 0 Å containing the $[Co_3Ge_3]$ ring. The calculations were performed at the PBE0/def2-TZVP level of theory, without including solvent effects.

https://doi.org/10.1021/jacs.4c16401
J. Am. Chem. Soc. XXXX, XXX, XXX−XXX

long-range shielding cone is obtained, which results from the spherical aromatic behavior ascribed to each building unit, in line with the spherical aromatic characteristics enabling shielding cone characteristics from any orientation of the external field. The NICS results are supported by intense diatropic ring currents inside each Ge_3Sn_6 unit (Figures 4b and S42). These ring currents[85−88] involve the whole cluster rather than being localized in the $[Co_3Ge_3]$ or $[Ge_3]$ rings, providing additional evidence that the delocalization is global. Interestingly, the ring currents are especially intense around the $[Ge_3]$ ring. Hence, the $[Co_3@Ge_6Sn_{18}]^{5-}$ cluster features three spherical aromatic units, which are connected to a giant σ-aromatic counterpart of triatomic σ-aromatic H_3^+ and Li_3^+ species.[17−22] This observation suggests the plausible finding of cluster-of-cluster analogs to discrete all-metal aromatic species, such as Al_4^{2-}, among others.[89]

Lastly, we evaluated the contribution from the core and valence electron manifold to dissect the shielding/deshielding patterns given exclusively by the above-discussed bonding elements. This enables an evaluation of core and valence electron contributions, favoring a clearer use of magnetic criteria of aromaticity in metallic clusters.[90,91] To this end, the recently proposed removing valence electron approximation is employed, unraveling contribution from core electrons,[92] which is obtained as a short-ranged deshielding pattern nearby atoms, which in turn contribute to a lesser extent in the overall shielding characteristics discussed above. In contrast, the valence electron manifold, featuring bonding elements ascribing an aromatic behavior to the characterized giant σ-aromatic cluster, enables a shielding response at the center of the structure and at each constituent unit, with the respective deshielding contour, leading to shielding cone characteristics, in line with its overall aromatic behavior (Figure 5). As to the

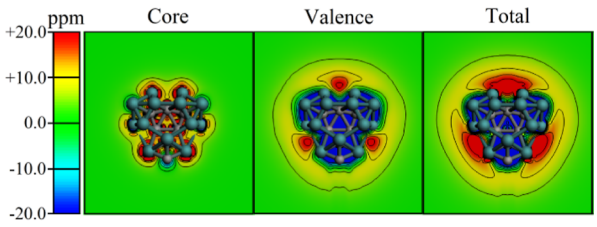

Figure 5. Contour plot representation of B_z^{ind}, in terms of the given contributions from both core and valence electron manifolds.

ring currents, the use of an all-electron basis set does not change the result obtained with pseudopotentials. However, using an all-electron basis set, the intensity of the ring currents around the $[Ge_3]$ ring is reduced, and the ring currents are somewhat more disorganized (Figure S43). We consider that the magnetic response gives a better account of aromaticity if the effect of core electrons is not included.[91]

CONCLUSIONS

In summary, the first Ge−Sn-mixed trimer, $[Co_3@Ge_6Sn_{18}]^{5-}$, was successfully characterized. The cluster is best described as $[Co_3^{3-}@Ge_6Sn_{18}^{2-}]$, featuring a 2e σ bond across the entire structure. Theoretical studies further revealed the global aromatic nature of the trimer. This discovery not only broadens the structural diversity of heteroatomic clusters but also extends the concept of σ-aromaticity, laying the groundwork for synthesizing larger σ-aromatic clusters. The successful synthesis of such aromatic multinuclear clusters advances our understanding of chemical bonding, paving the way for the rational design of new materials with desirable properties inspired by prototypical molecules.

ASSOCIATED CONTENT

Supporting Information

The Supporting Information is available free of charge at https://pubs.acs.org/doi/10.1021/jacs.4c16401.

Detailed experimental procedures, crystallographic supplementation, electrospray−ionization mass spectrometry (ESI−MS), energy-dispersive X-ray spectroscopic analysis, and quantum-chemical studies (PDF)) (PDF)

The data that support the findings of this study are available free of charge on the ACS Publications Web site.

Accession Codes

Deposition number 2341055 contains the supplementary crystallographic data for this paper. These data can be obtained free of charge via the joint Cambridge Crystallographic Data Centre (CCDC) and Fachinformationszentrum Karlsruhe Access Structures service.

AUTHOR INFORMATION

Corresponding Author

Zhong-Ming Sun − *State Key Laboratory of Elemento-Organic Chemistry, Tianjin Key Lab for Rare Earth Materials and Applications, School of Materials Science and Engineering, Nankai University, Tianjin 300350, China;* orcid.org/0000-0003-2894-6327; Email: sunlab@nankai.edu.cn

Authors

Ya-Shan Huang − *State Key Laboratory of Elemento-Organic Chemistry, Tianjin Key Lab for Rare Earth Materials and Applications, School of Materials Science and Engineering, Nankai University, Tianjin 300350, China*

Hong-Lei Xu − *State Key Laboratory of Elemento-Organic Chemistry, Tianjin Key Lab for Rare Earth Materials and Applications, School of Materials Science and Engineering, Nankai University, Tianjin 300350, China*

Wen-Juan Tian − *Institute of Molecular Science, Shanxi University, Taiyuan 030006, China;* orcid.org/0000-0002-1715-9216

Zi-Sheng Li − *State Key Laboratory of Elemento-Organic Chemistry, Tianjin Key Lab for Rare Earth Materials and Applications, School of Materials Science and Engineering, Nankai University, Tianjin 300350, China;* orcid.org/0000-0002-8545-9640

Sílvia Escayola − *Institut de Química Computacional i Catàlisi and Departament de Química, Universitat de Girona, Girona 17003 Catalonia, Spain; Institute for Theoretical Chemistry, University of Stuttgart, Stuttgart 70569, Germany*

Miquel Solà − *Institut de Química Computacional i Catàlisi and Departament de Química, Universitat de Girona, Girona 17003 Catalonia, Spain;* orcid.org/0000-0002-1917-7450

Alvaro Muñoz-Castro − *Facultad de Ingeniería, Arquitectura y Diseño, Universidad San Sebastián, Santiago 8420524, Chile;* orcid.org/0000-0001-5949-9449

Complete contact information is available at:

https://doi.org/10.1021/jacs.4c16401
J. Am. Chem. Soc. XXXX, XXX, XXX−XXX

https://pubs.acs.org/10.1021/jacs.4c16401

Author Contributions

The manuscript was written through the contributions of all the authors.

Notes

The authors declare no competing financial interest.

■ ACKNOWLEDGMENTS

This work was supported by the National Natural Science Foundation of China (nos. 22425107, 92461303, and 22371140). W.J.T. thanks financial support from the National Natural Science Foundation of China (22402108). A.M.-C. Thanks FONDECYT ANID Regular 1221676. M.S. is grateful for financial support from the Agencia Española de Investigación (MCIN/AEI/10.13039/501100011033) for project PID2023-147424NB-I00 and from the Generalitat de Catalunya for project 2021SGR623 and 2024 ICREA Academia prize. S.E. thanks the Alexander von Humboldt Foundation for a postdoctoral fellowship.

■ REFERENCES

(1) Kekulé, A. Sur la constitution des substances aromatiques. *Bull. Soc. Chim.* **1865**, *3*, 98−110.
(2) Faraday, M. On new compounds of carbon and hydrogen and on certain other products obtained during the decomposition of oil by heat. *Phil. Trans. Roy. Soc. Lond.* **1825**, *115*, 440−446.
(3) Merino, G.; Solà, M. Celebrating the 150th anniversary of the Kekulé benzene structure. *Phys. Chem. Chem. Phys.* **2016**, *18*, 11587−11588.
(4) Solà, M. Aromaticity rules. *Nat. Chem.* **2022**, *14*, 585−590.
(5) Dewar, M. J. S. σ-conjugation and σ-aromaticity. *Bull. Soc. Chim. Belg.* **1979**, *88*, 957−967.
(6) Dewar, M. J. S.; McKee, M. L. Aspects of cyclic conjugation. *Pure Appl. Chem.* **1980**, *52*, 1431−1441.
(7) Wang, M.; Wang, Y. Advances for Triangular and sandwich-shaped all-metal aromatics. *Molecules* **2024**, *29*, 763−803.
(8) Liu, C.; Popov, I. A.; Chen, Z.; Boldyrev, A. I.; Sun, Z. M. Aromaticity and antiaromaticity in Zintl clusters. *Chem.—Eur. J.* **2018**, *24*, 14583−14597.
(9) Popov, I. A.; Starikova, A. A.; Steglenko, D. V.; Boldyrev, A. I. Usefulness of the σ-aromaticity and σ-antiaromaticity concepts for clusters and solid-state compounds. *Chem.—Eur. J.* **2018**, *24*, 292−305.
(10) Galeev, T. R.; Boldyrev, A. I. Recent advances in aromaticity and antiaromaticity in transition-metal systems. *Annu. Rep. Prog. Chem., Sect. C: Phys. Chem.* **2011**, *107*, 124−147.
(11) Feixas, F.; Matito, E.; Poater, J.; Solà, M. Metalloaromaticity. *Wiley Interdiscip. Rev.: Comput. Mol. Sci.* **2013**, *3*, 105−122.
(12) Chen, Z.; King, R. B. Spherical aromaticity: recent work on fullerenes, polyhedral boranes, and related structures. *Chem. Rev.* **2005**, *105*, 3613−3642.
(13) Cui, P.; Hu, H. S.; Zhao, B.; Miller, J. T.; Cheng, P.; Li, J. A multicentre-bonded $[Zn^{I}]_8$ cluster with cubic aromaticity. *Nat. Commun.* **2015**, *6*, 6331−6335.
(14) El Bakouri, O.; Szczepanik, D. W.; Jorner, K.; Ayub, R.; Bultinck, P.; Solà, M.; Ottosson, H. Three-dimensional fully π-conjugated macrocycles: when 3D-aromatic and when 2D-aromatic-in-3D? *J. Am. Chem. Soc.* **2022**, *144*, 8560−8575.
(15) Mercero, J. M.; Boldyrev, A. I.; Merino, G.; Ugalde, J. M. Recent developments and future prospects of all-metal aromatic compounds. *Chem. Soc. Rev.* **2015**, *44*, 6519−6534.
(16) Zhao, J.; Du, Q.; Zhou, S.; Kumar, V. Endohedrally doped cage clusters. *Chem. Rev.* **2020**, *120*, 9021−9163.
(17) Oka, T. Chemistry, astronomy and physics of H_3^+. *Philos. Trans. A Math. Phys. Eng. Sci.* **2012**, *370*, 4991−5000.
(18) Oka, T. Interstellar H_3^+. *Chem. Rev.* **2013**, *113*, 8738−8761.
(19) Alexandrova, A. N.; Boldyrev, A. I. σ-Aromaticity and σ-antiaromaticity in alkali metal and alkaline earth metal small clusters. *J. Phys. Chem. A* **2003**, *107*, 554−560.
(20) Havenith, R. W. A.; De Proft, F.; Fowler, P. W.; Geerlings, P. σ-Aromaticity in H_3^+ and Li_3^+: insights from ring-current maps. *Chem. Phys. Lett.* **2005**, *407*, 391−396.
(21) Solà, M.; Boldyrev, A. I.; Cyrański, M. K.; Krygowski, T. M.; Merino, G. *σ-, π-, δ-, and ϕ-aromaticity in Aromaticity and Antiaromaticity: Concepts and Applications*; John Wiley & Sons, Chichester, 2023; Chapter 11, pp 207−222.
(22) Chakraborty, A.; Giri, S.; Chattaraj, P. K. Trapping of noble gases (He−Kr) by the aromatic H_3^+ and Li_3^+ species: a conceptual DFT approach. *New J. Chem.* **2010**, *34*, 1936−1945.
(23) Moses, M. J.; Fettinger, J. C.; Eichhorn, B. W. Interpenetrating As_{20} fullerene and Ni_{12} icosahedra in the onion-skin $[As@Ni_{12}@As_{20}]^{3-}$ ion. *Science* **2003**, *300*, 778−780.
(24) Li, Z.; Ruan, H.; Wang, L.; Liu, C.; Xu, L. Counterion-induced crystallization of intermetalloid Matryoshka clusters $[Sb@Pd_{12}@Sb_{20}]^{3-,4-}$. *Dalton Trans.* **2017**, *46*, 3453−3456.
(25) Wang, Y.; Moses-DeBusk, M.; Stevens, L.; Hu, J.; Zavalij, P.; Bowen, K.; Dunlap, B. I.; Glaser, E. R.; Eichhorn, B. $Sb@Ni_{12}@Sb_{20}^{\mp}$and $Sb@Pd_{12}@Sb_{20}^{n}$ cluster anions, where n = + 1,−1,−3,−4: multioxidation-state clusters of interpenetrating platonic solids. *J. Am. Chem. Soc.* **2017**, *139*, 619−622.
(26) Stegmaier, S.; Fässler, T. F. A bronze matryoshka: the discrete intermetalloid cluster $[Sn@Cu_{12}@Sn_{20}]^{12-}$ in the ternary phases $A_{12}Cu_{12}Sn_{21}$ (A = Na, K). *J. Am. Chem. Soc.* **2011**, *133*, 19758−19768.
(27) Shu, C. C.; Szczepanik, D. W.; Muñoz-Castro, A.; Solà, M.; Sun, Z. M. $[K_2(Bi@Pd_{12}@Bi_{20})]^{4-}$: An endohedral inorganic fullerene with spherical aromaticity. *J. Am. Chem. Soc.* **2024**, *146*, 14166−14173.
(28) Xu, Y. H.; Tian, W. J.; Muñoz-Castro, A.; Frenking, G.; Sun, Z. M. An all-metal fullerene: $[K@Au_{12}Sb_{20}]^{5-}$. *Science* **2023**, *382*, 840−843.
(29) Hirsch, A.; Chen, Z.; Jiao, H. Spherical aromaticity in I_h symmetrical fullerenes: the $2(N+1)^2$ rule. *Angew. Chem., Int. Ed.* **2000**, *39*, 3915−3917.
(30) Robilotto, T. J.; Bacsa, J.; Gray, T. G.; Sadighi, J. P. Synthesis of a trigold monocation: an isolobal analogue of $[H_3]^+$. *Angew. Chem., Int. Ed.* **2012**, *51*, 12077−12080.
(31) Freitag, K.; Gemel, C.; Jerabek, P.; Oppel, I. M.; Seidel, R. W.; Frenking, G.; Banh, H.; Dilchert, K.; Fischer, R. A. The σ-Aromatic Clusters $[Zn_3]^+$ and $[Zn_2Cu]$: Embryonic Brass. *Angew. Chem., Int. Ed.* **2015**, *54*, 4370−4374.
(32) Yadav, R.; Maiti, A.; Schorpp, M.; Graf, J.; Weigend, F.; Greb, L. Supramolecular trapping of a cationic all-metal σ-aromatic $\{Bi_4\}$ ring. *Nat. Chem.* **2024**, *16*, 1523−1530.
(33) Yong, L.; Wu, S. D.; Chi, X. X. Theoretical study of aromaticity in small hydrogen and metal cation clusters X_3^+ (X = H, Li, Na, K, and Cu). *Int. J. Quantum Chem.* **2007**, *107*, 722−728.
(34) Feixas, F.; Matito, E.; Duran, M.; Poater, J.; Solà, M. Aromaticity and electronic delocalization in all-metal clusters with single, double, and triple aromatic character. *Theor. Chem. Acc.* **2011**, *128*, 419−431.
(35) Boronski, J. T.; Seed, J. A.; Hunger, D.; Woodward, A. W.; van Slageren, J.; Wooles, A. J.; Natrajan, L. S.; Kaltsoyannis, N.; Liddle, S. T. A crystalline tri-thorium cluster with σ-aromatic metal-metal bonding. *Nature* **2021**, *598*, 72−75.
(36) Cuyacot, B. J. R.; Foroutan-Nejad, C. $[\{Th(C_8H_8)Cl_2\}_3]^{2-}$ is stable but not aromatic. *Nature* **2022**, *603*, E18−E20.
(37) Lin, X.; Mo, Y. On the bonding nature in the crystalline tri-thorium cluster: core-shell syngenetic sigma-aromaticity. *Angew. Chem., Int. Ed.* **2022**, *61*, No. e202209658.
(38) Szczepanik, D. W. Bonding in a crystalline tri-thorium cluster: not σ-aromatic but still unique. *Angew. Chem., Int. Ed.* **2022**, *61*, No. e202204337.
(39) Tomeček, J.; Liddle, S. T.; Kaltsoyannis, N. Actinide-actinide bonding: electron delocalisation and σ-aromaticity in the tri-thorium

cluster $[\{Th(\eta^8\text{-}C_8H_8)(\mu\text{-}Cl)_2\}_3K_2]$. *ChemPhysChem* **2023**, *24*, No. e202300366.
(40) Fedik, N.; Boldyrev, A. I.; Muñoz-Castro, A. Aromatic character of $[Au_{13}]^{5+}$ and $[MAu_{12}]^{4+/6+}$(M= Pd, Pt) cores in ligand protected gold nanoclusters−interplay between spherical and planar σ-aromatics. *Phys. Chem. Chem. Phys.* **2019**, *21*, 25215−25219.
(41) Popov, I. A.; Pan, F. X.; You, X. R.; Li, L. J.; Matito, E.; Liu, C.; Zhai, H. J.; Sun, Z. M.; Boldyrev, A. I. Peculiar all-metal σ-aromaticity of the $[Au_2Sb_{16}]^{4-}$ anion in the solid state. *Angew. Chem., Int. Ed.* **2016**, *55*, 15344−15346.
(42) Pan, F. X.; Xu, C. Q.; Li, L. J.; Min, X.; Wang, J. Q.; Li, J.; Zhai, H. J.; Sun, Z. M. A niobium-necked cluster $[As_3Nb(As_3Sn_3)]^{3-}$ with aromatic Sn_3^{2-}. *Dalton Trans.* **2016**, *45*, 3874−3879.
(43) Xu, Y. H.; Tkachenko, N. V.; Popov, I. A.; Qiao, L.; Muñoz-Castro, A.; Boldyrev, A. I.; Sun, Z. M. Ternary aromatic and anti-aromatic clusters derived from the hypho species $[Sn_2Sb_5]^{3-}$. *Nat. Commun.* **2021**, *12*, 4465−4472.
(44) Xu, H. L.; Tkachenko, N. V.; Szczepanik, D. W.; Popov, I. A.; Muñoz-Castro, A.; Boldyrev, A. I.; Sun, Z. M. Symmetry collapse due to the presence of multiple local aromaticity in Ge_{24}^{4-}. *Nat. Commun.* **2022**, *13*, 2149−2156.
(45) Xu, H. L.; Tkachenko, N. V.; Wang, Z. C.; Chen, W. X.; Qiao, L.; Muñoz-Castro, A.; Boldyrev, A. I.; Sun, Z. M. A sandwich-type cluster containing Ge@Pd_3 planar fragment flanked by aromatic nonagermanide caps. *Nat. Commun.* **2020**, *11*, 5286−5293.
(46) Tkachenko, N. V.; Chen, W. X.; Morgan, H. W.; Muñoz-Castro, A.; Boldyrev, A. I.; Sun, Z. M. Sn_{36}^{8-}: a 2.7 nm naked aromatic tin rod. *Chem. Commun.* **2022**, *58*, 6223−6226.
(47) Tkachenko, N. V.; Boldyrev, A. I. Multiple local σ-aromaticity of nonagermanide clusters. *Chem. Sci.* **2019**, *10*, 5761−5765.
(48) Wilson, R. J.; Lichtenberger, N.; Weinert, B.; Dehnen, S. Intermetalloid and heterometallic clusters combining p-block (semi) metals with d-or f-block metals. *Chem. Rev.* **2019**, *119*, 8506−8554.
(49) Wang, Y.; McGrady, J. E.; Sun, Z. M. Solution-based group 14 Zintl anions: new frontiers and discoveries. *Chem. Res.* **2021**, *54*, 1506−1516.
(50) Xu, H. L.; Qiao, L.; Sun, Z. M. Orientational isomerism and its reactivity of a main group sandwich anion $[Ge_9\text{-In-}Ge_9]^{5-}$. *Chin. J. Chem.* **2023**, *41*, 2432−2438.
(51) Huang, Y. S.; Xue, Y.; Muñoz-Castro, A.; Popov, I. A.; Sun, Z. M. $[Nb@Ge_{13/14}]^{3-}$: New family members of Ge-based intermetalloid clusters. *Chem.—Eur. J.* **2022**, *28*, No. e202202192.
(52) Huang, Y. S.; Chen, D.; Zhu, J.; Sun, Z. M. $[(CrGe_9)\text{-}Cr_2(CO)_{13}]^{4-}$: A disubstituted case of ten-vertex closo cluster with spherical aromaticity. *Chin. Chem. Lett.* **2022**, *33*, 2139−2142.
(53) Waibel, M.; Raudaschl-Sieber, G.; Fässler, T. F. Mixed tetrahedral Zintl clusters: single crystal structure determination of $[Si_{4-x}Ge_x]^{4-}$, $[(MesCu)_2(Si_{4-x}Ge_x)]^{4-}$, and the ^{29}Si MAS NMR spectra of $A_4Si_2Ge_2$ (A= K, Rb). *Chem.—Eur. J.* **2011**, *17*, 13391−13394.
(54) Gillett-Kunnath, M. M.; Petrov, I.; Sevov, S. C. Heteroatomic deltahedral zintl ions of group 14 and their alkenylation. *Inorg. Chem.* **2010**, *49*, 721−729.
(55) Gillett-Kunnath, M. M.; Muñoz-Castro, A.; Sevov, S. C. Trimetallic deltahedral Zintl ions: experimental and theoretical studies of the novel dimer $[(Sn_6Ge_2Bi)_2]^{4-}$. *Chem. Commun.* **2012**, *48*, 3524−3526.
(56) Gillett-Kunnath, M. M.; Paik, J. I.; Jensen, S. M.; Taylor, J. D.; Sevov, S. C. Metal-centered deltahedral zintl ions: Synthesis of [Ni@Sn_9]$^{4-}$ by direct extraction from intermetallic precursors and of the vertex-fused dimer $[\{Ni@Sn_8(\mu\text{-}Ge)_{1/2}\}_2]^{4-}$. *Inorg. Chem.* **2011**, *50*, 11695−11701.
(57) Hlukhyy, V.; He, H.; Jantke, L. A.; Fässler, T. F. The neat ternary solid $K_{5-x}Co_{1-x}Sn_9$ with endohedral $[Co@Sn_9]^{5-}$ cluster units: a precursor for soluble intermetalloid $[Co_2@Sn_{17}]^{5-}$ clusters. *Chem.—Eur. J.* **2012**, *18*, 12000−12007.
(58) Hlukhyy, V.; Stegmaier, S.; van Wüllen, L.; Fässler, T. F. Endohedrally filled $[Ni@Sn_9]^{4-}$ and $[Co@Sn_9]^{5-}$ clusters in the neat solids $Na_{12}Ni_{1-x}Sn_{17}$ and $K_{13-x}Co_{1-x}Sn_{17}$: crystal structure and ^{119}Sn solid-state NMR spectroscopy. *Chem.—Eur. J.* **2014**, *20*, 12157−12164.
(59) Pauling, L. Atomic radii and interatomic distances in metals. *J. Am. Chem. Soc.* **1947**, *69*, 542−553.
(60) Pyykkö, P.; Atsumi, M. Molecular single-bond covalent radii for elements 1−118. *Chem.—Eur. J.* **2009**, *15*, 186−197.
(61) Liu, C.; Popov, I. A.; Li, L. J.; Li, N.; Boldyrev, A. I.; Sun, Z. M. $[Co_2@Ge_{16}]^{4-}$: localized versus delocalized bonding in two isomeric intermetalloid clusters. *Chem.—Eur. J.* **2018**, *24*, 699−705.
(62) Witzel, B. J.; Klein, W.; Dums, J. V.; Boyko, M.; Fässler, T. F. Metallocages for metal anions: Highly charged $[Co@Ge_9]^{5-}$ and [Ru@ Sn_9]$^{6-}$ clusters featuring spherically encapsulated Co^{1-} and Ru^{2-} anions. *Angew. Chem., Int. Ed.* **2019**, *58*, 12908−12913.
(63) Wang, J. Q.; Stegmaier, S.; Fässler, T. F. $[Co@Ge_{10}]^{3-}$: An intermetalloid cluster with archimedean pentagonal prismatic structure. *Angew. Chem., Int. Ed.* **2009**, *48*, 1998−2002.
(64) Esenturk, E. N.; Fettinger, J. C.; Eichhorn, B. W. Synthesis, structure, and dynamic properties of $[Ni_2Sn_{17}]^{4-}$. *J. Am. Chem. Soc.* **2006**, *128*, 12−13.
(65) Bentlohner, M. M.; Jantke, L. A.; Henneberger, T.; Fischer, C.; Mayer, K.; Klein, W.; Fässler, T. F. On the nature of bridging metal atoms in intermetalloid clusters: synthesis and structure of the metal-atom-bridged Zintl clusters $[Sn(Ge_9)_2]^{4-}$ and $[Zn(Ge_9)_2]^{6-}$. *Chem.—Eur. J.* **2016**, *22*, 13946−13952.
(66) Wilson, R. J.; Broeckaert, L.; Spitzer, F.; Weigend, F.; Dehnen, S. $\{[CuSn_5Sb_3]^{2-}\}_2$: a dimer of inhomogeneous superatoms. *Angew. Chem., Int. Ed.* **2016**, *55*, 11775−11780.
(67) Xu, L.; Sevov, S. C. Oxidative coupling of deltahedral $[Ge_9]^{4-}$ Zintl ions. *J. Am. Chem. Soc.* **1999**, *121*, 9245−9246.
(68) Ugrinov, A.; Sevov, S. C. $[Ge_9{-}Ge_9{-}Ge_9]^{6-}$: A linear trimer of 27 germanium atoms. *J. Am. Chem. Soc.* **2002**, *124*, 10990−10991.
(69) Ekardt, W. Work function of small metal particles: Self-consistent spherical jellium-background model. *Phys. Rev. B: Condens. Matter Mater. Phys.* **1984**, *29*, 1558−1564.
(70) Cohen, M. L.; Chou, M. Y.; Knight, W. D.; De Heer, W. A. Physics of metal clusters. *J. Phys. Chem.* **1987**, *91*, 3141−3149.
(71) de Heer, W. A. The physics of simple metal clusters: experimental aspects and simple models. *Rev. Mod. Phys.* **1993**, *65*, 611−676.
(72) Muñoz-Castro, A. $[Ba_4@Sn_{56}]^{36-}$ as a main-group second-order superatom. interpenetrated dodecahedrons as a three-dimensional cluster-of-clusters structure. *Inorg. Chem.* **2024**, *63*, 20102−20107.
(73) Teo, B. K. Cluster of clusters: A new series of high nuclearity Au-Ag clusters. *Polyhedron* **1988**, *7*, 2317−2320.
(74) Foster, J. M.; Boys, S. Canonical configurational interaction procedure. *Rev. Mod. Phys.* **1960**, *32*, 300−302.
(75) Szczepanik, D. W.; Andrzejak, M.; Dominikowska, J.; Pawełek, B.; Krygowski, T. M.; Szatylowicz, H.; Solà, M. The Electron Density of Delocalized Bonds (EDDB) Applied for Quantifying Aromaticity. *Phys. Chem. Chem. Phys.* **2017**, *19*, 28970−28981.
(76) Szczepanik, D. W.; Andrzejak, M.; Dyduch, K.; Żak, E.; Makowski, M.; Mazur, G.; Mrozek, J. A Uniform Approach to the Description of Multicenter Bonding. *Phys. Chem. Chem. Phys.* **2014**, *16*, 20514−20523.
(77) Szczepanik, D. W.; Żak, E.; Dyduch, K.; Mrozek, J. Electron Delocalization Index Based on Bond Order Orbitals. *Chem. Phys. Lett.* **2014**, *593*, 154−159.
(78) Islas, R.; Heine, T.; Merino, G. The induced magnetic field. *Acc. Chem. Res.* **2012**, *45*, 215−228.
(79) Merino, G.; Heine, T.; Seifert, G. The Induced Magnetic Field in Cyclic Molecules. *Chem.—Eur. J.* **2004**, *10*, 4367−4371.
(80) Chen, Z.; Wannere, C. S.; Corminboeuf, C.; Puchta, R.; Schleyer, P. v. R. Nucleus-Independent Chemical Shifts (NICS) as an Aromaticity Criterion. *Chem. Rev.* **2005**, *105*, 3842−3888.
(81) Fliegl, H.; Taubert, S.; Lehtonen, O.; Sundholm, D. The Gauge Including Magnetically Induced Current Method. *Phys. Chem. Chem. Phys.* **2011**, *13*, 20500−20518.

https://doi.org/10.1021/jacs.4c16401
J. Am. Chem. Soc. XXXX, XXX, XXX−XXX

(82) Sundholm, D.; Fliegl, H.; Berger, R. J. F. Calculations of Magnetically Induced Current Densities: Theory and Applications. *Wiley Interdiscip. Rev. Comput. Mol. Sci.* **2016**, *6*, 639−678.
(83) Schleyer, P. v. R.; Maerker, C.; Dransfeld, A.; Jiao, H.; van Eikema Hommes, N. J. R. Nucleus-Independent Chemical Shifts: A Simple and Efficient Aromaticity Probe. *J. Am. Chem. Soc.* **1996**, *118*, 6317−6318.
(84) Merino, G.; Solà, M.; Fernández, I.; Foroutan-Nejad, C.; Lazzeretti, P.; Frenking, G.; Anderson, H. L.; Sundholm, D.; Cossío, F. P.; Petrukhina, M. A.; Wu, J.; Wu, J. I.; Restrepo, A. Aromaticity: Quo Vadis. *Chem. Sci.* **2023**, *14*, 5569−5576.
(85) Monaco, G.; Zanasi, R. AACID: Anisotropy of the Asymmetric Magnetically Induced Current Density Tensor. *J. Phys. Chem. A* **2018**, *122*, 4681−4686.
(86) Sundholm, D.; Dimitrova, M.; Berger, R. J. F. Current density and molecular magnetic properties. *Chem. Commun.* **2021**, *57*, 12362−12378.
(87) Badri, Z.; Foroutan-Nejad, C. On the aromaticity of actinide compounds. *Nat. Rev. Chem.* **2024**, *8*, 551−560.
(88) Lazzeretti, P. Ring currents. *Prog. Nucl. Magn. Reson. Spectrosc.* **2000**, *36*, 1−88.
(89) Li, X.; Kuznetsov, A. E.; Zhang, H. F.; Boldyrev, A. I.; Wang, L. S. Observation of all-metal aromatic molecules. *Science* **2001**, *291*, 859−861.
(90) Munoz-Castro, A. Magnetic response properties of coinage metal macrocyles. Insights into the induced magnetic field through the analysis of $[Cu_5(Mes)_5]$, $[Ag_4(Mes)_4]$, and $[Au_5(Mes)_5]$(Mes= 2, 4, 6-Me3C6H2). *J. Phys. Chem. C* **2012**, *116*, 17197−17203.
(91) Orozco-Ic, M.; Soriano-Agueda, L.; Sundholm, D.; Matito, E.; Merino, G. Core-electron contributions to the magnetic response of molecules with heavy elements and their significance in aromaticity assessments. *Chem. Sci.* **2024**, *15*, 12906−12921.
(92) Orozco-Ic, M.; Charistos, N. D.; Muñoz-Castro, A.; Islas, R.; Sundholm, D.; Merino, G. Core-electron contributions to the molecular magnetic response. *Phys. Chem. Chem. Phys.* **2022**, *24*, 12158−12166.

https://doi.org/10.1021/jacs.4c16401
J. Am. Chem. Soc. XXXX, XXX, XXX−XXX